Journal of Materials Science & Technology 33 (2017) 1004–1008

Contents lists available at ScienceDirect

Journal of Materials Science & Technology

journal homepage: www.jmst.org

Friction stir welding of carbon nanotubes reinforced Al-Cu-Mg alloy composite plates

Ke Zhao, Zhenyu Liu, Bolyu Xiao*, Zongyi Ma

Shenyang National Laboratory for Materials Science, Institute of Metal Research, Chinese Academy of Sciences, Shenyang 110016, China

ARTICLE INFO

Article history:
Received 8 December 2016
Received in revised form
16 December 2016
Accepted 20 December 2016
Available online 31 January 2017

Keywords:
Carbon nanotubes
Metal matrix composites
Friction stir welding

ABSTRACT

Carbon nanotubes (CNTs) reinforced Al-Cu-Mg composite plates of 2.2 mm in thickness after extrusion and T4 treatment were joined by friction stir welding (FSW) and the joint efficiency reaches 87%. There was no precipitate in both heat-affected zone (HAZ) and nugget zone (NZ) as a medium rotation rate of 800 rpm and a relative high travel speed of 100 mm min^{-1} were used. In the NZ, FSW disarranged the alignment of CNTs to random orientation and dispersed CNT uniformly. The orientation of CNTs perpendicular to the tensile direction and the possible dissolution of solute clusters made the HAZ become the weakest zone in the joint leading to the failure in the HAZ.

1. Introduction

Compared to aluminum alloys, discontinuously reinforced aluminum matrix composites (DRAs) with increased strength and stiffness are widely used in aerospace industry [1–3]. SiC, B_4C, Al_2O_3 or other particles with micron-size are commonly used as the reinforcements [3–6]. Unfortunately, the machining capability of the composites is much reduced due to addition of the hard ceramic particles [7]. Furthermore, the strength increment by these micro-sized particles is not pronounced [8–11]. It is believed that nano-sized reinforcements can overcome the above problems [3,12].

With extremely high mechanical properties, carbon nanotubes (CNTs) have attracted much attention as an ideal reinforcement for the DRAs [9,13,14]. Significantly improved modulus, strength, and wear resistance make CNT reinforced aluminum (CNT/Al) composites a new generation of DRAs. Previous efforts were mainly focused on fabrication of CNT/Al composites with superior properties [3,15,16]. However, little attention was paid on welding of CNT/Al composites, which is important for a wide application of CNT/Al composites.

Friction stir welding (FSW), a novel solid-state joining technique, is widely used for welding of aluminum alloys [17]. High-quality FSW joints without fusion welding defects could be easily obtained because no melting and solidification processes occurred [18]. Furthermore, FSW has been proven to be feasible for joining of DRAs, such as Al_2O_3/Al, SiCp/Al, B_4C/Al composites [5,6,19,20]. However, severe wear of steel tool caused by hard ceramic particles occurred during FSW [21,22]. Even the cemented carbide and cermet tools were used and the tool wear could not be completely avoided [17,22]. This restricted application of FSW in joining of DRAs.

Considering the nanoscale size and flexibility of CNTs, the CNT/Al composites are expected to exhibit good weldability and have not severe tool wear. Unfortunately, to the best knowledge of the authors, no attempts of joining CNT/Al composites by FSW have been made so far.

For heat-treatable aluminum alloys and DRAs, heat affected zone (HAZ) is usually the weakest zone due to dissolution or coarsening of precipitates [17,23]. Furthermore, different from the aluminum alloys and DRAs reinforced by particles, the CNT/Al composites behave obvious anisotropy because CNTs with a large aspect ratio are directionally aligned. Complicated plastic flow during FSW will change the orientation of CNTs in the nugget zone (NZ), which might weaken the NZ [7]. Therefore, it is of practical importance to understand the microstructure evolutions in different zones of CNT/Al composites during FSW.

In this study, a steel tool with threaded conical shaped pin was used to join the CNT/2009Al composite plates. Microstructure evolutions including CNT distribution, CNT length, grain size and precipitated phase in different zones of the joints were investigated. The aim is to obtain high joint efficiency in CNT/Al composites.

* Corresponding author.
E-mail address: blxiao@imr.ac.cn (B. Xiao).

http://dx.doi.org/10.1016/j.jmst.2017.01.033
1005-0302/

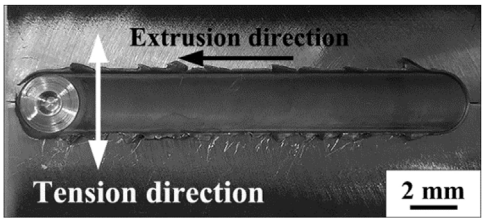

Fig. 1. Macrograph of FSW CNT/2009Al composite.

2. Experimental

The as-received CNTs provided by Tsinghua University had entangled morphologies with an outer diameter of 10–20 nm. 3 vol.% CNTs were ball milled with 2009Al alloy (Al–4 wt.% Cu-1.5 wt.% Mg) powders in an attritor at 400 rpm for 6 h. The as-milled powders were cold-compacted in a cylinder die under a pressure of about 10 MPa, degassed and subsequently hot pressed into billet. The billet was finally hot-extruded into a bar with 30 mm in diameter. Composite plates with a thickness of 2.2 mm were machined from the extruded bar and then subjected to T4 treatment (solution treated at 770 K for 2 h, water quenched, and naturally aged for 7 d).

A steel tool was used for friction stir welding which has a concave shoulder of 14 mm in diameter and a threaded conical shaped pin of 1.7 mm in length. The diameters of conical pin at the root and head were 4.70 mm and 4.17 mm, respectively. The composite plates were butt-welded at a rotation rate of 800 rpm and a travel speed of 100 mm min^{-1}. The welding direction was parallel to the extrusion direction. After welding the joint were naturally aged for 7 d.

Optical microscopic (OM) examination and hardness measurement were carried out on the cross-sectional surface of the joint. The Vickers hardness was measured along the mid-thickness of the joint with an interval of 0.5 mm by an automatic testing machine (LECO, LM-247AT) under a load of 100 g for 15 s. The microstructures of the joint and based material (BM) were characterized by transmission electron microscopy (TEM, Tecnai F20).

Tensile specimens with a gauge length of 40 mm and a width of 8 mm were machined perpendicular to the welding direction with the NZ in the center of the gauge. Five tensile specimens were tested at a strain rate of 10^{-3} s^{-1} using a tensile tester (Shimadzu AG-100KNG).

3. Results and discussion

3.1. Tensile properties and hardness

Fig. 1 shows the macroscopic morphology of the FSW joint of CNT/2009Al composite. The surface of the joint was smooth and no macro-defects were detected, which indicated that sound joint of CNT/2009Al composite was achieved.

Table 1 shows ultimate tensile strength (UTS) of the BM and the FSW joint. The UTS of the BM attained 630 MPa due to strengthening of CNT and refined grain. However, the elongation (EL) of the BM was only 1%, which was attributed to the anisotropy of CNT/Al composites. The tension direction was perpendicular to the CNT alignment direction, leading to lower ductility [7]. The UTS of the FSW joint was 550 MPa, exhibiting a joint efficiency of 87%.

Table 1
Tensile properties of CNT/2009Al and the as-welded joint (YS: yield strength; EL: elongation).

Sample	YS (MPa)	UTS (MPa)	EL (%)
BM	610	630	1
Joint	500	550	1

Fig. 2(a) shows the OM image of the CNT/2009Al composite joint. No void or CNT cluster was observed, implying sound joint of CNT/2009Al composite. An obvious basin-shaped NZ with a bottom width of 8 mm and top width of 14 mm can be seen, which is much larger than the pin diameter of 4.7 mm. This is attributed to thermal-mechanical effect of shoulder. As the thickness of welded plates was only about 2.2 mm, the effect of shoulder was significant, resulting in greatly increased NZ width.

Fig. 2(b) shows the hardness profile of the joint. Compared to the hardness of the BM (208 HV on average), the hardness of the weld was significantly reduced. However, no obvious low hardness zone was observed throughout the whole weld. While the HAZ on the retreating side exhibited an unapparent low-hardness zone with a hardness value of about 175 HV, the NZ showed a slightly fluctuated hardness distribution with a low hardness of about 175 HV on the retreating side.

All tensile specimens of the joint fractured at the HAZ on the retreating side, as shown in Fig. 2(c). It was interesting to note that no specimens fractured at the NZ, although it had a similar hardness to the HAZ in which fracture occurred.

3.2. Microstructures

Fig. 3(a)–(c) shows the CNT distributions in different zones of FSW joint. As shown in Fig. 3(a) and (b), most of CNTs in the BM and the HAZ were aligned along the welding direction, i.e. the extrusion direction. However, the CNT orientation in the NZ was changed to random distribution (Fig. 3(c)), which can be attributed to the complicated plastic flow during FSW [15]. The small white points shown in Fig. 3(c) corresponded to CNTs which were perpendicular to the welding direction. The CNTs in the NZ were all homogenously dispersed, no re-clustering of CNTs occurred during the FSW process.

Despite severe deformation in the NZ, a perfect tubular structure of CNTs was retained, as shown in Fig. 4(a) and (b). However, a decrease in length of CNTs was observed in the NZ. The average length of CNTs deceased from about 150 nm to about 80 nm based on TEM observations. As orientation of CNTs was random in the NZ, the CNT length under observation was about 3/5 (planar random) of the actual length. According to this, the actual CNT length in the NZ should be about 135 nm. This indicates that the CNT length was reduced by FSW, and this result was in agreement with our previous study [24].

Fig. 5(a), (c) and (e) show the matrix grains at different joint zones. The BM had an average grain size of about 200 nm (Fig. 5(a)). After welding, the grain size in the HAZ changed little (Fig. 5(c)). This

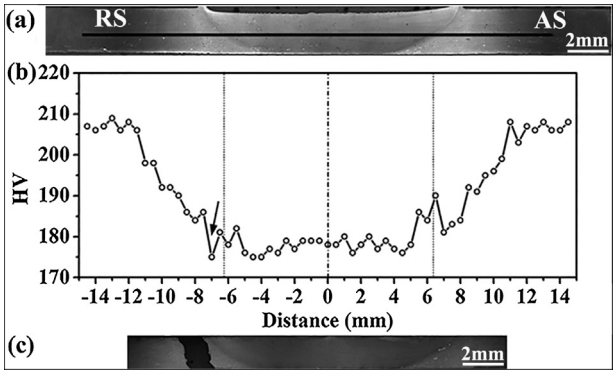

Fig. 2. (a) Cross-sectional macrostructure, (b) micro-hardness profiles of FSW CNT/2009Al joint (Arrows corresponding to the fracture site in HAZ), and (c) macrostructure of failed joint after tension (RS: retreating side; AS: advancing side).

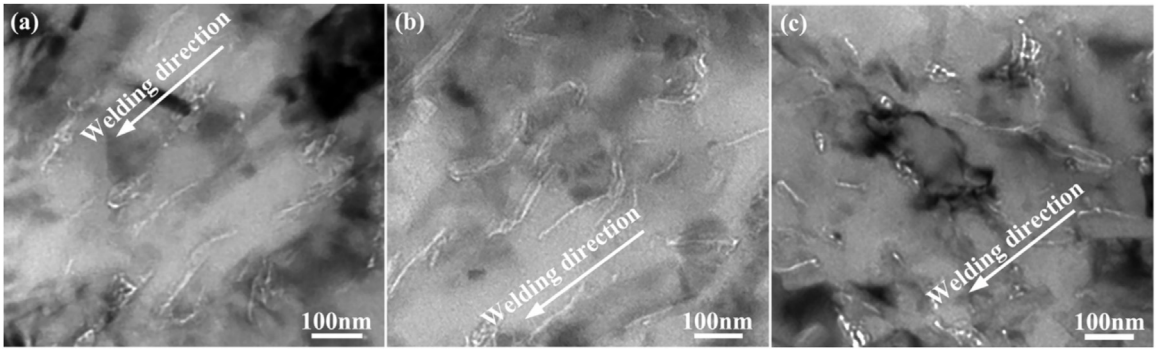

Fig. 3. TEM images showing CNT distribution in (a) BM, (b) HAZ and (c) NZ of FSW CNT/2009Al joint.

was attributed to the effective pinning of CNTs on the grain boundaries. It was reported that the grains of CNT/Al composite could keep stable when annealing at 723 K [25]. However, the average grain size in the NZ coarsened to about 400 nm (Fig. 5(e)), which could be attributed to the combination of heat input and serious deformation during FSW [15].

The precipitation sequence of 2009Al alloy is complicated and remains controversial [23]. It was generally recognized that the primary strengthening phases in the 2009Al were GPB (Guinier-Preston-Bagaryatsky) zones or clusters of solute atoms [26]. It was also reported that SiCp/2009Al composite were mainly strengthened by the clusters of solute atoms after natural aging [27–29]. The GPB zones of the composite were indiscernible under conventional TEM, while they could be detected by diffusion streaks in the diffraction patterns [30,31].

As shown in Fig. 5(b), no precipitate was observed in the BM and the selected area electron diffraction (SAED) patterns taken in a <100> zone axis indicated that GPB zones did not exist in the BM. This suggested that the CNT/2009Al composite was mainly strengthened by the clusters of solute atoms. Similarly, no precipitates were observed in the HAZ and NZ, and the diffraction patterns showed there were also no GPB zones in the HAZ and NZ, as shown in Fig. 5(d) and (f).

It has been reported that partial dissolution of GPB zones and solute clusters occurred at temperature ranging from 393 to 508 K for Al-Cu or Al-Cu-Mg alloy [26]. According to Zhang et al.'s research [23], the thermal cycle with a peak temperature of 508 K dissolved the solute clusters in the HAZ of FSW joint of 2024Al-T351. The present CNT/Al plates were welded using the same welding parameters as that in Ref. [23], it is believed that similar thermal cycle occurred during the FSW process, resulting in the dissolution of the solute clusters in the HAZ and NZ. Compared to Ref. [23], the present CNT/2009Al composite plates were thinner. Therefore, the NZ and HAZ cooled to room temperature rapidly after FSW, leading to a short duration of thermal cycle. As a result, precipitating process could be suppressed.

3.3. *Factors influencing mechanical properties*

Three possible factors, grain size, precipitate phase and reinforcement, greatly affect the hardness in different zones of joint. Firstly, the grains in the NZ were coarsened while the grains in the HAZ and the BM remained invariant, leading to the hardness decrease in the NZ. Secondly, the dissolution of the solute atoms clusters in the HAZ and the NZ also had a negative effect on their micro-hardness [23]. Thirdly, CNTs in the BM and the HAZ were aligned while the CNTs in the NZ were randomly oriented. The micro-hardness testing could be considered as micro compression test along the welding direction, i.e. the extrusion direction. That implied that hardness contribution from CNTs in the NZ was the lowest compared with that in the BM and the HAZ during micro-hardness testing. The above three factors led to that the HAZ and NZ exhibited similar hardness.

One fact should be mentioned that the tensile properties of the joint was tested perpendicular to the welding direction, however,

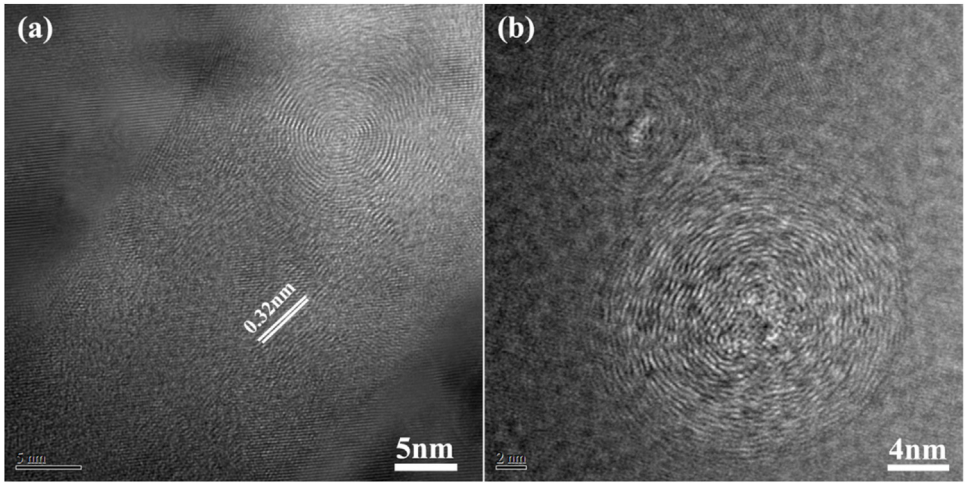

Fig. 4. Longitudinal (a) and cross-sectional (b) HRTEM images of CNTs in NZ.

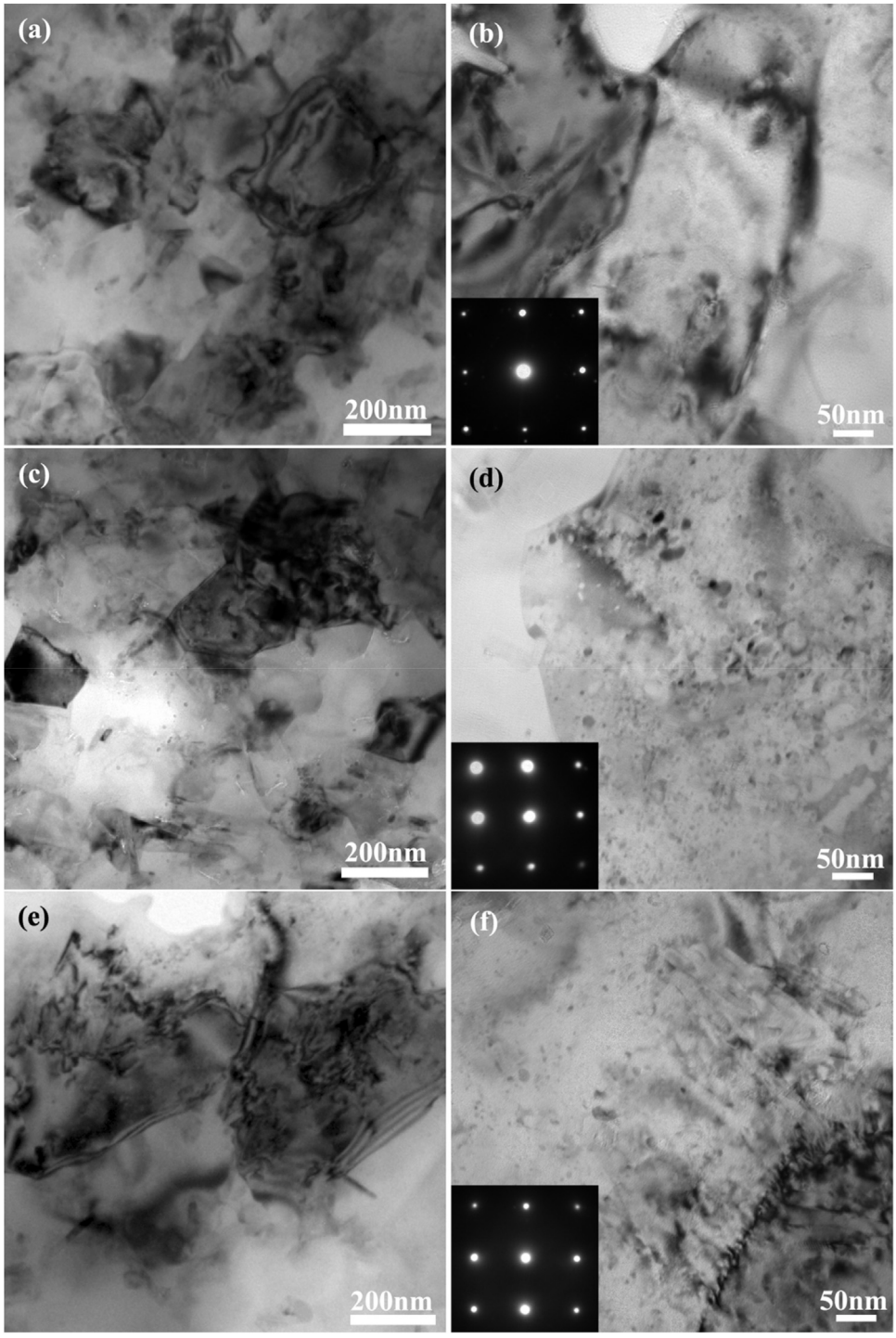

Fig. 5. TEM (a, c, e) images and bright-field micrographs (b, d, f) of grains in BM (a, b), HAZ (c, d) and NZ (e, f) of FSW CNT/2009Al joint (The insets correspond to the SAED patterns of <100> zone axis of BM, HAZ and NZ, respectively).

the micro-hardness were compressed along the welding direction. Therefore, the micro-hardness values did not totally correspond to the tensile properties along the tensile direction because of the different CNT orientation types. When the tension was perpendicular to the welding direction, the load transfer strengthening due to CNTs in the NZ with random CNT distribution was much stronger than that in the HAZ where most of CNTs were aligned to be perpendicular to the tensile direction. This explains why all specimens of the joint fractured at the HAZ rather than the NZ, although the NZ and the HAZ had similar hardness.

4. Conclusions

(1) 3 vol.% CNT/2009Al composite plates with 2.2 mm in thickness was successfully joined by FSW at a rotation rate of 800 rpm and a travel speed of 100 mm min^{-1}. No macro-defects were observed, and FSW joint with high welding efficiency of 87% was achieved.

(2) FSW resulted in the random orientation of CNTs in the NZ. No precipitate was detected in the HAZ and the NZ. The HAZ on the retreating side was the weakest zone due to the adverse CNT

orientation and possible dissolution of solute clusters. Therefore, the FSW joint fractured at the HAZ.

Acknowledgments

The authors gratefully acknowledge the support of the National Basic Research Program of China under grant Nos. 2011CB932603 and 2012CB619600, the CAS/SAFEA International Partnership Program for Creative Research Teams and the National Natural Science Foundation of China under grant No.51501189.

References

[1] D.B. Miracle, Compos. Sci. Technol. 65 (2005) 2526–2540.
[2] J.W. Kaczmar, K. Pietrzak, W. Wlosinski, J. Mater. Process. Technol. 106 (2000) 58–67.
[3] S.R. Bakshi, D. Lahiri, A. Agarwal, Int. Mater. Rev. 55 (2010) 41–64.
[4] A.B. Pandey, B.S. Majumbar, D.B. Miracle, Acta Mater. 49 (2001) 405–417.
[5] X.G. Chen, M. da Silva, P. Gougeon, L. St-Georges, Mater. Sci. Eng. A 518 (2009) 174–184.
[6] J.M. Root, D.P. Field, T.W. Nelson, Metall. Mater. Trans. A 40 (2009) 2109–2114.
[7] Z.Y. Liu, B.L. Xiao, W.G. Wang, Z.Y. Ma, Acta Metall. Sin. (Engl. Lett.) 27 (2014) 901–908.
[8] J.M. Torralba, C.E. da Costa, F. Velasco, J. Mater. Process. Technol. 133 (2003) 203–206.
[9] W.A. Curtin, B.W. Sheldon, Mater. Today 7 (11) (2004) 44–49.
[10] A.M.K. Esawi, M.M. Farag, Mater. Des. 28 (2007) 2394–2401.
[11] E. Neubauer, M. Kitzmantel, M. Hulman, P. Angerer, Compos. Sci. Technol. 70 (2010) 2228–2236.
[12] T.S. Chin, Mater. Sci. Eng. R 74 (2013) 281–350.
[13] P.M. Ajayan, O.Z. Zhou, Top. Appl. Phys. 80 (2001) 391–425.
[14] E.T. Thostenson, Z. Ren, T.W. Chou, Compos. Sci. Technol. 61 (2001) 1899–1912.
[15] Z.Y. Liu, B.L. Xiao, W.G. Wang, Z.Y. Ma, Carbon 62 (2013) 35–42.
[16] Z.Y. Liu, K. Zhao, B.L. Xiao, W.G. Wang, Z.Y. Ma, Mater. Des. 97 (2016) 424–430.
[17] R.S. Mishra, Z.Y. Ma, Mater. Sci. Eng. R 50 (2005) 1–78.
[18] Z. Zhang, B.L. Xiao, Z.Y. Ma, Mater. Charact. 106 (2015) 255–265.
[19] D. Wang, B.L. Xiao, Q.Z. Wang, Z.Y. Ma, Mater. Des. 47 (2013) 243–247.
[20] D.R. Ni, D.L. Chen, D. Wang, B.L. Xiao, Z.Y. Ma, Mater. Des. 51 (2013) 199–205.
[21] R.A. Prado, L.E. Murr, D.J. Shindo, K.F. Soto, Scr. Mater. 45 (2001) 75–80.
[22] D.J. Shindo, A.R. Rivera, L.E. Murr, J. Mater. Sci. 37 (2002) 4999–5005.
[23] Z. Zhang, B.L. Xiao, Z.Y. Ma, Acta Mater. 73 (2014) 227–239.
[24] Z.Y. Liu, B.L. Xiao, W.G. Wang, Z.Y. Ma, Carbon 69 (2014) 264–274.
[25] J. Lipecka, M. Andrzejczuk, M. Lewandowska, J. Janczak-Rusch, K.J. Kurzydłowski, Compos. Sci. Technol. 71 (2011) 1881–1885.
[26] G. Sha, R.K.W. Marceau, X. Gao, B.C. Muddle, S.P. Ringer, Acta Mater. 59 (2011) 1659–1670.
[27] R.K.W. Marceau, G. Sha, R.N. Lumley, S.P. Ringer, Acta Mater. 58 (2010) 1795–1805.
[28] P. Rodrigo, P. Poza, V. Utrilla, A. Ureña, J. Alloys Compd. 479 (2009) 451–456.
[29] D. Wang, Q.Z. Wang, B.L. Xiao, Z.Y. Ma, Mater. Sci. Eng. A 589 (2014) 271–274.
[30] S. Cheng, Y.H. Zhao, Y.T. Zhu, E. Ma, Acta Mater. 55 (2007) 5822–5832.
[31] M.J. Starink, S.C. Wang, F. Lefebvre, J.L. Yan, I. Sinclair, Mater. Sci. Eng. A 431 (2006) 123–136.